Talanta 251 (2023) 123757

Contents lists available at ScienceDirect

Talanta

journal homepage: www.elsevier.com/locate/talanta

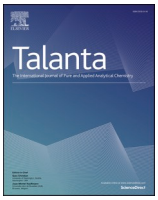

Comparison of Mg/Ca concentration series from *Patella depressa* limpet shells using CF-LIBS and LA-ICP-MS

Marina Martínez-Minchero [a,b,*], Adolfo Cobo [a,b,c,d], Ana Méndez-Vicente [e], Jorge Pisonero [f], Nerea Bordel [f], Igor Gutiérrez-Zugasti [d], Patrick Roberts [g,h], Álvaro Arrizabalaga [i], José Valdiande [a], Jesús Mirapeix [a,b,c], José Miguel López-Higuera [a,b,c], Asier García-Escárzaga [g,i,j,**]

[a] *Photonics Engineering Group, Universidad de Cantabria, Spain*
[b] *Instituto de Investigación Sanitaria Valdecilla (IDIVAL), Spain*
[c] *CIBER-BBN, Instituto de Salud Carlos III, 28029, Madrid, Spain*
[d] *Instituto Internacional de Investigaciones Prehistóricas de Cantabria (Universidad de Cantabria, Gobierno de Cantabria, Banco Santander), Univ. de Cantabria, Spain*
[e] *Servicios Científico-Técnicos, Unidad de Ensayos Medioambientales. Universidad de Oviedo, Spain*
[f] *Departamento de Física, Universidad de Oviedo, Spain*
[g] *Department of Archaeology, Max Planck Institute for the Science of Human History, Germany*
[h] *School of Social Sciences, University of Queensland, Queensland, Australia*
[i] *Departamento de Geografía, Prehistoria y Arqueología, Universidad Del País Vasco (UPV/EHU), Spain*
[j] *Department of Prehistory and Institute of Environmental Science and Technology (ICTA), Universitat Autònoma de Barcelona, Bellaterra, Spain*

ARTICLE INFO

Keywords:
CFLIBS
LA-ICP-MS
LIBS
Mg/Ca profiles
Archaeology
Mollusk shells
Paleoclimate

ABSTRACT

The elemental composition of marine mollusk shells can offer valuable information about environmental conditions experienced by a mollusk during its lifespan. Previous studies have shown significant correlations between Mg/Ca concentration ratios measured on biogenic carbonate of mollusk shells and sea surface temperature (SST). Here we propose the use of Laser-Induced Breakdown Spectroscopy (LIBS) and the validation of the Calibration-Free LIBS (CF-LIBS) approach for the rapid measurement and estimation of Mg/Ca molar concentration profiles within *Patella depressa* Pennant, 1777 limpet shells. To achieve these objectives, results derived from CF-LIBS methodology are compared with those obtained from an established analytical technique for this purpose, such as Laser Ablation Inductively Coupled Plasma Mass Spectrometry (LA-ICP-MS). Concentration series obtained with both methodologies show defined temporal patterns and reflect the season-of-capture in each specimen. The results evidence a significant correlation ($R^2 = 0.63–0.81$) between CF-LIBS and LA-ICP-MS Mg/Ca molar concentration profiles within four live-collected *P. depressa* shells. Averaged error for the molar concentration estimated with CF-LIBS was lower than 10% in every specimen. The comparison between the results obtained from two techniques used in this study has allowed us to demonstrate for the first time that Mg/Ca molar concentration measured in biogenic carbonates were accurately inferred using CF-LIBS technique. The CF-LIBS approach validation represents great potential for the rapid and large-scale paleoenvironmental and archaeological analysis of this mollusk species, which is frequently found in archaeological sites.

1. Introduction

Marine mollusks have been exploited as a food resource by humans in the past; hence, their shells are frequently preserved and found in archaeological sites all over the world, from low to high latitudes [1–4]. Shell chemical composition can act as a powerful recorder of seasonal sea surface temperature (SST) variations experienced by a mollusk in the past, enabling researchers to reconstruct past climate conditions [5–7], as well as to accurately establish the period of the year when it died/was collected by humans [3,8–10]. The correlation between stable oxygen isotope ratios derived from biogenic carbonate ($\delta^{18}O$) and SST has been

* Corresponding author. Photonics Engineering Group, Universidad de Cantabria, Spain.
** Corresponding author. Department of Prehistory and Institute of Environmental Science and Technology (ICTA), Universitat Autònoma de Barcelona, Bellaterra, Spain
E-mail addresses: marina.martinez@unican.es (M. Martínez-Minchero), asier.garcia@uab.cat (A. García-Escárzaga).

https://doi.org/10.1016/j.talanta.2022.123757
Received 23 March 2022; Received in revised form 5 July 2022; Accepted 18 July 2022
Available online 4 August 2022

List of abbreviations

Ar	Argon
Ba	Barium
Ca	Calcium
CCD	Charge-coupled device
CF-LIBS	Calibration Free Laser Induced Breakdown Spectroscopy
ICP-MS	Inductively Coupled Plasma Mass Spectrometry
ICP-OES	Inductively Coupled Plasma Optical Emission Spectrometry
LA-ICP-MS	as Laser Ablation Inductively Coupled Plasma Mass Spectrometry
LTE	Local Thermodynamic Equilibrium
LIBS	Laser-Induced Breakdown Spectroscopy
Mg	Magnesium
mmol	milimol
Nd-YAG	Neodymium Doped Yttrium–Aluminum-Garnet
NIST	National Institute of Standards and Technology
SST	Sea Surface Temperature
Sr	Strontium

extensively demonstrated in previous works [11–13]. Although it is a very commonly used method in paleoclimatic and archaeological studies, oxygen isotope fractionation is influenced by oxygen isotope composition of the seawater ($\delta^{18}O_{sw}$) [14,15]. This poses a notable limitation for paleoreconstructions where the values for $\delta^{18}O_{sw}$ are unknown. This has motivated the development of independent paleotemperature proxies. A correlation between SST and the quantity of some trace elements (magnesium, strontium, etc.) incorporated into the biogenic calcium carbonate matrix has also been found for shells of certain species [16–18]. Indeed, trace element ratios of biogenic carbonates, most commonly Mg/Ca in biogenic calcite and Sr/Ca in aragonite, have been widely investigated as potential temperature proxies to serve as complements or alternatives to $\delta^{18}O$ carbonate analysis [19].

Laser-Induced Breakdown Spectroscopy (LIBS), an atomic spectroscopy technique based on the optical analysis of laser-generated plasmas from the sample material, has proven to be particularly promising in this regard thanks to its high thru-put. When a high-energy laser pulse is focused on the sample, a material ablation is produced, generating a plasma whose composition is proportional to the elemental concentration of the sample. The plasma emits optical radiation depending on the present elements, which enable their identification by their unique spectral signatures [20]. LIBS has been widely employed on a variety of materials and has seen a diversity of applications such as the analysis of metallic alloys [21–23], biomedicines [24,25], minerals and rocks [26–28], soils [29], as well as its use in forensic studies [30] and archaeology and cultural heritage [31–33]. LIBS offers multiple advantages over other analytical techniques including versatility, no contact requirements, multi-elemental analysis, it being practically non-destructive, and a reduction in, or lack of, sample preparation [34]. Measuring solid samples, such as mollusk shells, with the commonly used techniques for this purpose (ICP-OES or ICP-MS) requires micro-milled sampling procedures and subsequent acid digestion, which can be highly time-consuming compared to LIBS procedure which offers a number of benefits in the context of more limited sample preparation requirements, lower costs, and an increased rapidity in measurement and accumulation of data from multiple individuals from a given context [35–37]. Laser ablation-inductively coupled plasma-mass spectrometry (LA-ICP-MS) is a highly accepted and widely used technique for the analysis of major, minor and trace elements, as well as isotope-ratio determination [38–43]. Due to the use of laser ablation as a sampling method, this analytical technique combines the advantage of not requiring acid digestion of the sample with the advantages of ICP techniques related to precision and robustness. However, despite its good analytical performance, LA-ICP-MS suffers from very high cost and significant complexity when comparing both technologies. Therefore, LIBS offers more versatility, improved speed, ease of operation, affordability and portability [44]. Previous work has demonstrated that Mg/Ca ratios obtained along the growth axis of limpets using LIBS showed very well-defined seasonal cycles that correctly reflected the annual variations in SST [36,37,45–47]. However, one of the main issues with the LIBS technique is that the spectral line intensities from a given element are strongly dependent on the physical and chemical properties of the sample (the so-called matrix effect) [37]. For this reason, a reference material with almost identical properties to the sample should be used for calibration plots. Due to the absence of specific matrix-matched calibration standards for marine mollusk shell biogenic carbonates, previous studies employed two line emission intensities from LIBS spectra to obtain Mg/Ca values given in arbitrary units [36,46]. The use of line ratios can nevertheless lead to LIBS-derived variability due to changes in experimental conditions such as optical alignment, temperature or spectrometer configuration and variability between specimens. Molar concentration ratios of elements should provide significant advantages over the line ratio approach.

The calibration-free LIBS procedure (CF-LIBS) is a quantitative algorithmic method that allows the elemental concentration of materials to be obtained without the aforementioned matrix effect [48]. This is accomplished without the necessity for calibration curves or reference samples, and it is not affected by possible variations of experimental parameters such as laser energy, spot size, or sample roughness. This method appears to be suitable for analyzing samples with complex matrices for which matrix-matched standards are not available, e.g., rocks, minerals and meteorites [49–52] or archaeological artifacts [53–56]. This approach allows us to obtain relative concentrations in mmol/mol units. Nonetheless, it requires validation because CF-LIBS is an algorithm that relies on some assumptions about plasma characteristics, which may differ from real conditions. Therefore, the numerical concentration that we obtain must be checked against the actual values.

Previous works applying the CF-LIBS approach to marine mollusk shell biogenic carbonates highlighted the paleoenvironmental and archaeological potential of this novel methodology [37]. Nevertheless, additional study is still required to improve the algorithm tentatively used by García-Escárzaga et al. [37] to estimate Mg/Ca molar concentrations in biogenic carbonates. Here, therefore, we propose the validation of the Calibration-Free LIBS approach for the estimation of the molar ratios of both magnesium and calcium elements in *Patella depressa* Pennant, 1777 limpet shells. In order to validate the LIBS technique for this application, the molar ratio sequences have been compared to LA-ICP-MS measurements of the same shells. Confirmation of this technique would open up significant avenues for the rapid measurement of shells from archaeological and other contexts and the expansion of sample sizes used in the assessment of season of collection or past paleoclimate.

2. Materials and methods

2.1. Sample preparation

P. depressa limpet shells were live-collected at Langre Beach along the coast of Cantabria (North of Spain) in the month of September, which corresponds to the end of the warmer period of the year, i.e., the summer season. To form the marine mollusk shells, the carbonate precipitates in the form of growth increments from the apex to the shell edge. Preparation of the shells was carried out at the Institute of Prehistory (IIIPC) of the University of Cantabria (Spain). The shells were sectioned along the growth axis following the procedures applied in previous research on the same limpet species [37]. Four selected

samples were partially coated with an epoxy resin along the maximum growth axis to avoid the shell breaking when cut. Sectioning was performed using a Buehler Isomet low-speed saw and a diamond wheel. From each limpet, a 3 mm section was obtained (Fig. 1a).

The sections were fixed onto a glass microscope slide and ground on glass plates using 600 and 800 SiC grit powder and polished with a 1 μm diamond suspension grit until the internal growth lines and increments were clearly visible. The section was used for elemental analyses using LA-ICP-MS and LIBS on the calcite layer from the shell apex (the first portion of the shell growth) to the shell edge (the last portion of the shell growth) (Fig. 1b). The measurements were performed following a path in the calcite layer of the limpet, from the apex to the outer edge, crossing the growth lines. (Fig. 1c). (Supplementary Figs. 1–4).

2.2. LA-ICP-MS setup and analyses

LA-ICP-MS methodologies begin by ablating the sample material using a laser source; then, the ablated sample is ionized within the induced-coupled plasma (ICP) source. Once produced, the ions are detected and separated according to their m/z ratio. Quantification is based on comparative measurement using external reference materials and internal standardization. Sample analyses were accomplished at the University of Oviedo (Spain). The LA-ICP-MS setup (Fig. 2) consists of a laser ablation unit (193 nm ArF excimer laser - Analyte G2, Teledyne - Photon Machines-) coupled to a quadrupole mass spectrometer (model 7700x from Agilent Technologies).

The analyses were performed as transects (line scans) following limpet growth lines from the apex of the shell to the edge. Prior to analysis, a pre-ablation was carried out to clean the surface of the limpets. For this purpose, a slightly larger spot size and a higher ablation speed were employed. Experimental conditions are shown in Table 1.

The isotopes set in the method were ^{25}Mg, ^{43}Ca, ^{88}Sr and ^{137}Ba with an integration time (dwell time) of 100 ms for each isotope, resulting in a total acquisition time of 0.4 s. Under these conditions, at the set scanning speed, a lateral resolution of approximately 20 μm was obtained along the line trajectory.

ICP-MS analysis conditions were optimized by the ablation of the international reference standard NIST612 glass (fluence 5 J/cm^2, circular spot ∅ 85 μm, scan rate 5 μm/s, frequency 10 Hz), monitoring oxide production and plasma robustness by the ratios ^{248}ThO/^{232}Th (0.5%) and ^{238}U/^{232}Th (~1.15), respectively.

The international standard reference materials used for calibration were the synthetic glasses SRM 610 and 612 from The National Institute of Standards and Technology (NIST), as well as the MACS3 calcium carbonate standard reference from the U.S. Geological Survey (USGS). All standards were measured in triplicate at the beginning and end of the analytical session as well as every ~30 min to monitor sensitivity drift.

Data treatment and processing were performed with the assistance of Iolite4 software [57] taking MACS3 and the two NIST 610 and 612 standards as calibration and secondary standards, respectively. Elemental concentrations were expressed as mmol/mol in relation to calcium, which was selected as the internal standard element with a value of 40.4% weight.

2.3. LIBS setup and measurements

A selection of four *P. depressa* shell samples were measured using a LIBS setup at the University of Cantabria (Spain), after the performance of the LA-ICP-MS measurements and following the same path. The experimental setup (Fig. 3) comprises a pulsed laser source that produces the material ablation of the sample and a spectrometer to collect and analyze the light emitted from the plasma. The laser source is a Q-Switched Nd:YAG double-pulsed laser (Lotis LS-2134D) operating at a wavelength of 1064 nm, with 16 ns pulse width and 10 Hz repetition rate. The pulse energy was set to 35 mJ. The laser spot was focused with a lens of 75 mm focal length, producing a spot of 200 μm diameter and 0.2 μm depth (average) for each laser shot, resulting in an irradiance value at the sample surface approximately equal to 7 GW/cm^2. The light emitted from the plasma generated on the sample surface was captured by a collimating lens and conducted to the spectrometer through two optical fibers.

One was a fused silica, solarization resistant, optical fiber with 1 mm core diameter, coupled to another, which was made up of a bundle of eight optical fibers, each one with a 200 μm core diameter and a total diameter for the bundle of around 800 μm. The spectrometer used in this study is an eight-channel Avantes ULS2048-USB2-RM CCD spectrometer with a total wavelength range from 178 to 889 nm and a resolution from 0.015 to 0.06 nm. The collection of the plasma-emitted light was set to start 1 μs after the second laser pulse, with an acquisition gate of 1 ms (the minimum capture time for this non-gated spectrometer). A trough-lens vision system with a CCD camera allowed the inspection of the sample surface. The sample position was controlled by a motorized XYZ positioner, programmed to follow a measurement path along the shell surface.

In this experiment, the spectra acquisition was performed in the air at atmospheric pressure and ambient temperature. Measurements were made every 25 μm, and 12 consecutive laser pulses per point were recorded for averaging.

2.4. CF-LIBS application

The algorithm used is an implementation of the method originally proposed by Ciucci et al. [48]. The CF-LIBS approach is a quantitative methodology that produces accurate quantitative measurements of the elemental composition of a sample without using calibration curves and allows overcoming the matrix effect. For this purpose, some assumptions about the plasma conditions should be made. First, we assume that the ablation is stoichiometric, i.e., the plasma composition is representative of the actual composition of the sample before the ablation. In addition, we assume that the plasma is in local thermodynamic equilibrium (LTE) in the real-time and space observation window. Finally, the third assumption is that the plasma lines are optically thin. Another experimental requirement for the CF-LIBS is that the spectral range of measurement should include measurable lines from all the elements present

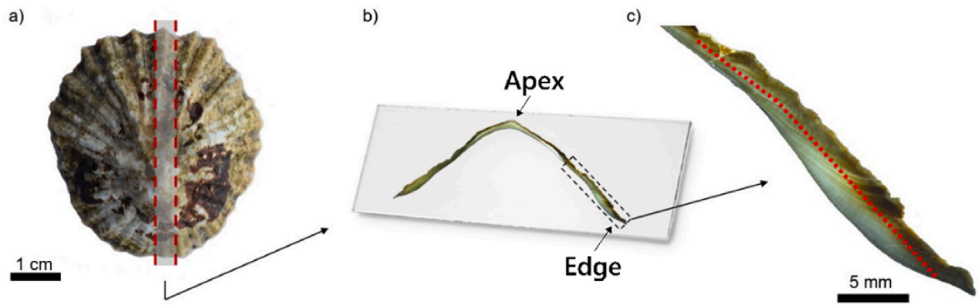

Fig. 1. Limpet sampling process.

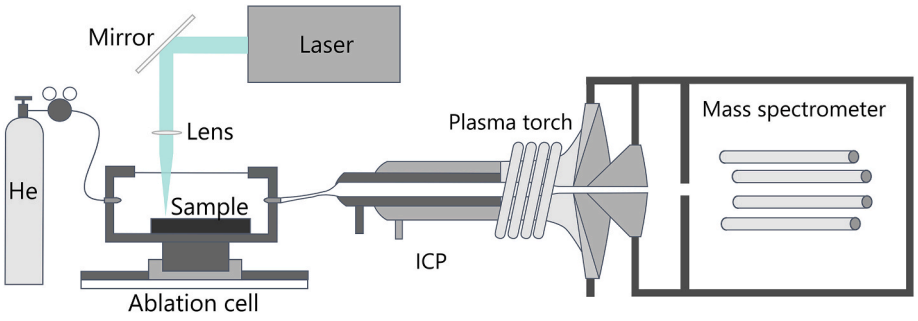

Fig. 2. LA-ICP-MS setup.

Table 1
LA-ICP-MS operating conditions.

Pre-ablation parameters	Ablation parameters	ICP parameters
Energy (fluence) = 2 J/cm^2 Pulse frequency = 10 Hz Spot size, diameter = 65 μm Scan speed = 200 μm/s	Energy (fluence) = 5 J/cm^2 Pulse frequency = 10 Hz Spot size, diameter = 30 μm Scan speed = 50 μm/s Cell gas (He) flow rate = 800 ml/min	RF Power = 1600 W Plasma gas (Ar) = 15 L/min Carrier gas (Ar) = 0.8 L/min Sample Depth = 4.3 mm

in the sample [58].

Based on LTE approximation, the line integral intensity corresponding to the transition levels E_k and E_i of an atomic species s is described in Eq. (1):

$$I^{ki} = FC_s A_{ki} \frac{g_k\, e^{-}(E_k/k_B T)}{U_s(T)} \tag{1}$$

where I^{ki} represents the measured integral line intensity; F is an experimental factor; C_s is the concentration of the emitting atomic species s; A_{ki} is the transition probability for the given line; g_k is the k level degeneracy; K_B is the Boltzmann constant; T is the plasma temperature, and $U_s(T)$ is the partition function for the emitting species at the plasma temperature. Applying logarithm to Eq. (1), we obtain:

$$ln\frac{I^{ki}}{g_k A_{ki}} = -\frac{E_k}{k_B T} + ln\frac{C_s F}{U_s(T)} \tag{2}$$

The equation can be written as a linear equation of the following form

$$y = mx + q_s$$

$$\text{where} \quad y = ln\frac{I^{ki}}{g_k A_{ki}},\ x = E_k\ ,\ m = -\frac{1}{k_B T}\ ,\ q_s = ln\frac{C_s F}{U_s(T)} \tag{3}$$

Using the definitions below and the parameters from the database, every measured line can be represented as a point in the 2D Boltzmann plane, which is the space identified by the x and y coordinates of Eq. (2). Every atomic species can be represented as parallel lines. The slope (m) of the lines obtained from the Boltzmann plot is related to the plasma temperature T, while the intercept (q_s) is related logarithmically to the species concentration C_s. From the intercept value, the concentration of the corresponding species can be calculated as follows:

$$C_s = \frac{1}{F} U_s(T) e^{q_s} \tag{4}$$

The experimental factor F can be obtained by normalizing the sum of the concentration of all the species to one:

$$\sum_s C_s = 1 \tag{5}$$

The linear fitting of each element must have very similar slopes,

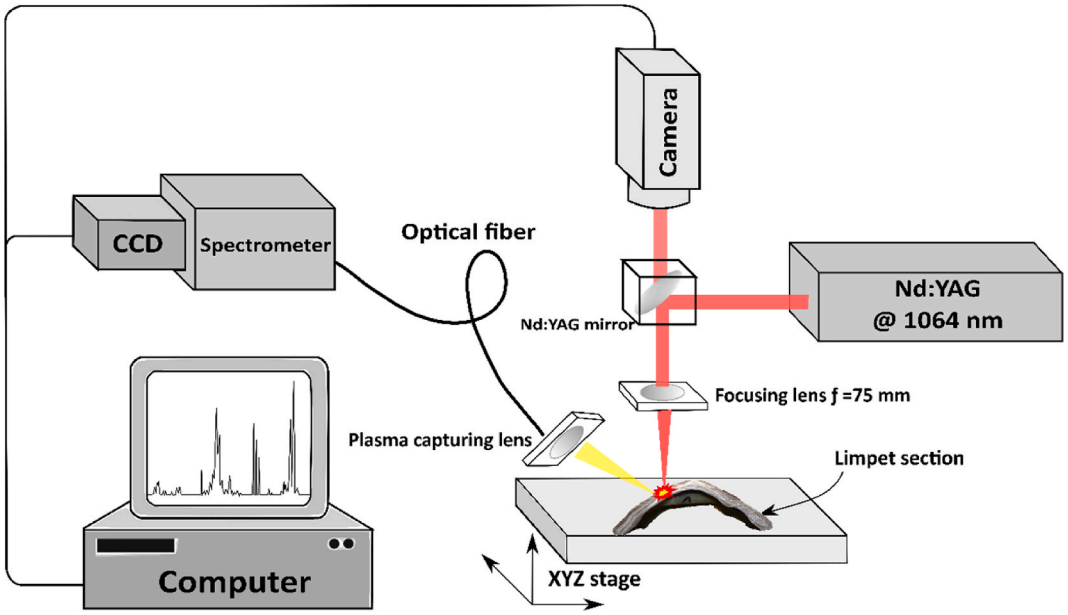

Fig. 3. LIBS setup used for spectra acquisition.

which means all the elements have the same temperature, and the plasma is in LTE. To obtain the value of the plasma temperature more accurately, a Saha–Boltzmann plot (combination of excitation Boltzmann distribution and Saha ionization distribution) must be used. In this method, emission lines from atoms and ions of the same element are included in the linear regression. The Saha ionization equation (Eq. (6)) shows the relation between the concentrations of neutral and ionic species for the same element.

$$\frac{C_{s\,II}F}{C_{s\,I}F} = 2\frac{U_{s\,II}(T)}{U_{s\,I}(T)}\frac{(2\pi m_e k_B T)^{\frac{3}{2}}}{N_e\,h^3}\,e^{-\left(\frac{E_{ion}}{k_B T}\right)} \tag{6}$$

Saha-Boltzmann plots can be explained as:

$$x = \left\{ E_k^I \quad for\ neutral\ lines\ E_k^{II} + E_{ion} \quad for\ ionic\ lines \right. \tag{7}$$

$$y = \left\{ ln\frac{I^{ki}}{g_k\,A_{ki}} \quad for\ neutral\ lines\ ln\frac{I^{ki}}{g_k\,A_{ki}} - ln\left(\frac{2(2\pi m_e k_B T)^{\frac{3}{2}}}{N_e\,h^3}\right) \quad for\ ionic\ lines \right. \tag{8}$$

In Eq. (6), E_{ion} represents the ionization energy; m_e is the mass of the electron, and N_e is the electron density. The electron density N_e can be obtained independently from measurements of Stark broadening.

To obtain accurate results from the CF-LIBS algorithm, the above-mentioned criteria must be fulfilled, mainly, LTE and optically thin conditions. For our experimental setup, with a non-gated spectrometer, verification of LTE conditions is a relevant issue, because the time integration window is always longer than the plasma lifetime, and only the capture delay from the laser shot can be accurately controlled. LTE conditions involve, on one hand, dominant collision processes over radiative ones, which are more easily matched at the beginning of the plasma evolution (shorter delays). On the other hand, the required small rate of variation of thermodynamic parameters of the plasma is better fulfilled at late stages (longer delays). As a compromise, we have chosen the reported value of 1 μs delay, a widely used value for CF-LIBS [58]. With this delay, the continuum background emission is reduced while the overall atomic emission is still high. In these conditions, the contribution to the optical emission spectrum of the much less intense plasma at later stages results in a "gated-like" operation with a shorter effective capture window, which further helps to achieve the LTE conditions [59]. In our experiments, we have verified that the Ca I and Mg I emission lines fall to 10% of intensity (with respect to their maximum value) at 6 μs after the laser shot, while Ca II and Mg II lines almost disappear after 2 μs. This suggests a "gated-like" operation with an equivalent temporal capturing window of 5 μs with 1 μs delay.

To assure that the emission lines entering the CF-LIBS algorithm are optically thin, a selection procedure has been implemented, following advice in Fu et al. [60]. First, an average spectrum from all measurements in each sample is analyzed, and the emission lines are identified. Selection of the suitable ones is based on line intensity, signal to background ratio, overlapping with lines of the same or different species, and isolation from other lines. For the surviving lines, their spectroscopic parameters (from NIST [61] and Genie databases [62]) have been considered: lower transition energy, transition probability, transition probability accuracy, availability of the Stark broadening parameter, and a wide range of upper energy levels for the Saha-Boltzmann plots.

3. Results and discussion

3.1. LA-ICP-MS concentration profiles

LA-ICP-MS data were firstly obtained, giving Mg/Ca concentration sequences along the growth axis. As the spot diameter of LA-ICP-MS measurements is approximately six times smaller than the LIBS crater (30 μm vs 200 μm), a rolling average for six data points was calculated to enable comparison of the concentration measurements of both techniques. The resulting sequences are smoother than the raw series, as seen in Fig. 4.

3.2. CF-LIBS approach results

A first step in the application of the CF-LIBS algorithm is the selection of suitable emission lines that will be used in the Saha-Boltzmann plots to calculate the plasma temperature, electronic density, and elemental concentration. With the criteria described in section 2.4, twelve emission lines (six from Ca and six from Mg) have been selected. As an important criterion in our application, selected lines should be available in all spatial points of the shell, so the same number of lines are used to create the Saha-Boltzmann plots in each one. This helps to reduce the variability of the ratio sequences. The selected lines are shown in Table 2, with the last column showing the value of the optical depth parameter k_t, which is related to the degree of self-absorption [58]. It must be noted that four of them are resonant lines (i.e., zero lower energy level) and the two Mg II lines have a high value of k_t, usually indicating that they are prone to self-absorption. In our experiments, however, we have found that these four resonant lines (two of them from Ca I and two from Mg II) are of very low intensity but high signal to noise ratio, and do not show apparent self-absorption, as the fitting error to an optically thin Lorentzian profile is lower than 7%. Their inclusion in the CF-LIBS algorithm result, in contrast, in a more stable ratio sequence and does not affect the concentration values significantly: removing the resonant lines modifies the concentration values by less than 2% while variability is much larger, due to the lower number of lines used in the Saha-Boltzmann plots.

Once LIBS spectra were recorded and lines selected, CF-LIBS calculations were performed along the shell growth axis of the four selected limpets. Temperature and electronic density were necessary to obtain Mg and Ca concentrations. Electronic density is obtained through the averaged Stark broadening of selected emission peaks. Saha-Boltzmann plots were represented for every limpet specimen in order to obtain plasma temperature (in Fig. 5 a Saha-Boltzmann plot for Mg and Ca corresponding to sample LAN.565 is shown). To assess the LTE conditions, the McWhirter criterion has been used [60]. Plasma temperatures obtained from the Saha-Boltzmann plots (see Table 3) are around 7500 K; from this, minimum electronic density to achieve LTE conditions should be 1.8E16 cm^{-3}, while our average value is 5.7E16cm^{-3}. As an additional necessary condition for LTE [58], we have verified that the diffusion length of a non-homogeneous, non-stationary plasma (calculated in our case as 0.025 mm) is much shorter than the variation length (with typical values of a few mm in our experimental conditions).

The calculations required to obtain the concentrations at each spatial point were carried out by a Matlab implementation of the CF-LIBS algorithm described before in section 2.4. The code is available at https://github.com/acobo/CFLIBS.

3.3. CF-LIBS and LA-ICP-MS comparison

The maximum and minimum values for the molar Mg/Ca concentration ratio (Table 4) were reasonably consistent between the four specimens and the techniques applied. Concentration ratio values obtained herein were largely similar to results previously measured on calcite carbonate on *Patella vulgata* Linnaeus, 1758 limpet species using the ICP-OES technique [36] (averaged minimum and maximum were 13.0 and 24.1 mmol Mg/mol Ca, respectively), and results from *Patella* spp. Limpets shells using ICP-MS [18] (averaged minimum and maximum Mg/Ca concentration ratios were 14.4 and 23.1 mmol/mol).

Moreover, concentration series obtained by both methods showed very well-defined temporal patterns covering warmer and colder periods. Mg/Ca concentration series calculated with CF-LIBS presents a good visual fit with the LA-ICP-MS profiles, as can be seen in Fig. 6.

Previous work, including research conducted on the species studied here [37], demonstrated that higher values in Mg/Ca ratios measured in

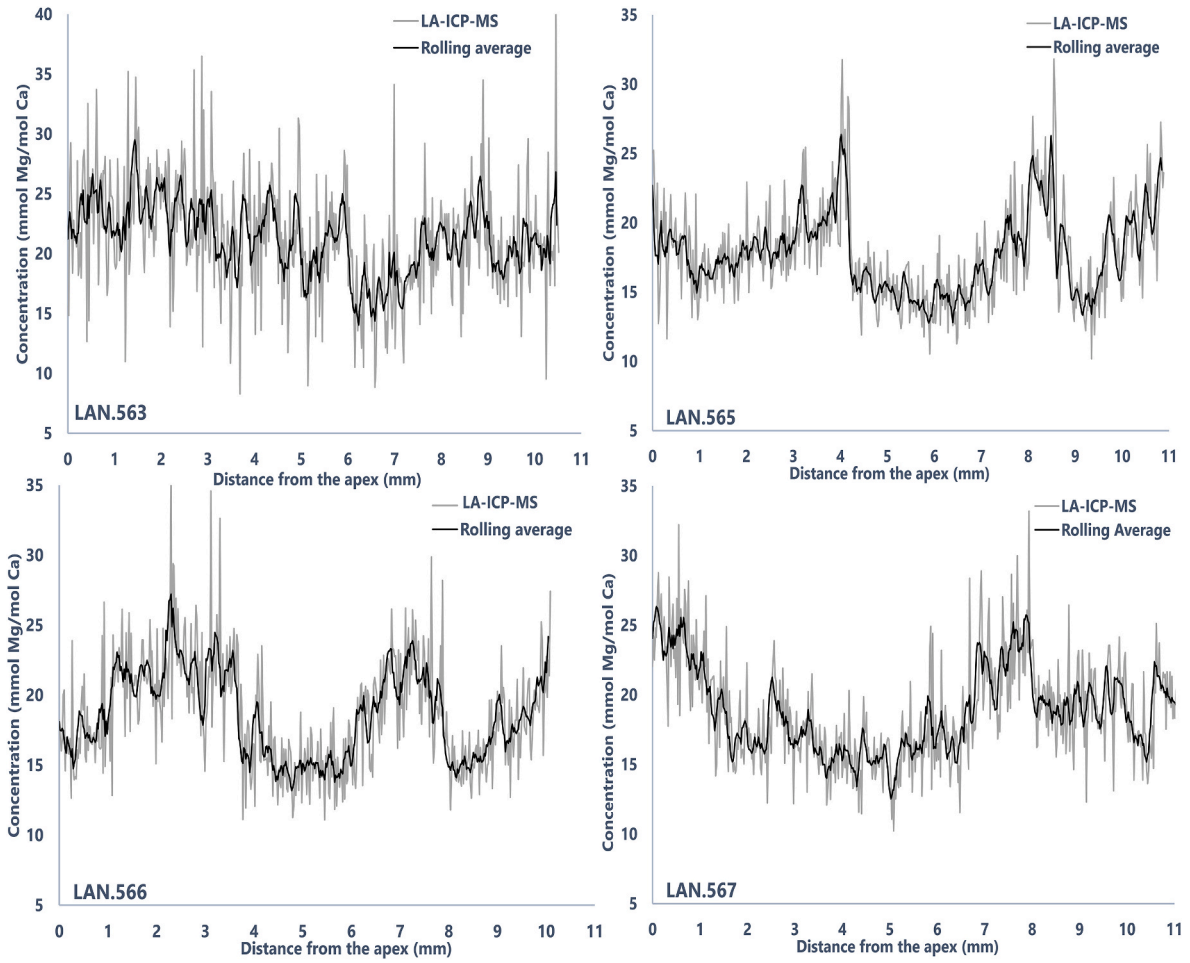

Fig. 4. Mg/Ca concentration values obtained with LA-ICP-MS procedure (grey line) compared to the same data applying a rolling average (black line).

Table 2
Spectroscopic parameters of neutral and ionized atomic lines of Ca and Mg used in CF-LIBS calculations. Data from NIST [61].

Element	Ionization	Wavelength (nm)	Aki(s^{-1}) × 10^8	gk	Ek (eV)	k_t
Ca	I	227.546	0.301	3	5.447	11.11
Ca	I	239.856	0.167	3	5.167	7.61
Ca	I	558.197	0.060	7	4.743	5.63
Ca	II	315.887	3.100	4	7.047	7.45
Ca	II	370.603	0.880	2	6.468	1.98
Ca	II	373.690	1.700	2	6.468	3.86
Mg	I	382.935	0.899	3	5.946	14.84
Mg	I	516.732	0.113	3	5.108	5.99
Mg	I	517.268	0.339	3	5.108	17.96
Mg	I	518.360	0.561	3	5.108	24.04
Mg	II	279.553	2.600	4	4.434	415.30
Mg	II	280.270	2.570	2	4.422	208.03

marine mollusk shells are related to higher SST, and lower values in Mg/Ca ratios suggest lower SST [36,47]. Here, for both analytical techniques, the four specimens show a high Mg/Ca value at the end of the sequence (far right portion of the Mg/Ca ratio series) where the edge of the shell is located (i.e. the most recently formed part of the limpet). As these specimens were collected at the end of the summer, this data correctly reflects the season of capture (high SST). Limpets LAN.565, LAN.566 and LAN.567 clearly show seasonal cycles in the concentration series (Fig. 6b, c, and 6d). By contrast, the sequence of the limpet LAN.563 shows a less clear sinusoidal trend in both, the LIBS and LA-ICP-MS measurement series (Fig. 6a). The different behavior on the

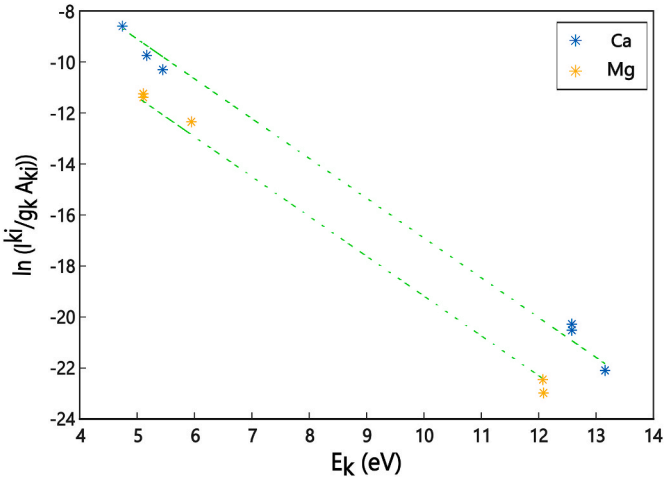

Fig. 5. Saha-Boltzmann plot for limpet LAN.565 for the elements Ca and Mg.

Table 3
Plasma temperature of the limpets analyzed.

Sample	LAN.563	LAN.565	LAN.566	LAN.567
Te (K)	7445 ± 111	7506 ± 100	7374 ± 110	7414 ± 136

Table 4
Maximum and minimum Mg/Ca relative concentration results from CF-LIBS and LA-ICP-MS for the four mollusk shell samples.

Sample	LAN.563	LAN.565	LAN.566	LAN.567
Maximum CF-LIBS (mmol Mg/mol Ca)	25.6	27.4	26.1	27.7
Minimum CF-LIBS (mmol Mg/mol Ca)	15.1	14.1	14.8	14.2
Maximum LA-ICP-MS (mmol Mg/mol Ca)	29.5	26.4	27.2	26.3
Minimum LA-ICP-MS (mmol Mg/mol Ca)	14.0	12.8	13.2	12.5

Mg/Ca series in this specimen is unknown, but several studies suggest that the magnesium incorporation to the calcite shell may depend on factors other than temperature and may even be variable within the same species [63]. Physiological processes involved in shell formation may change throughout its growth and introduce impurities and heterogeneities in its composition [64,65] due to factors such as stress, metabolic activity or control of shell crystal elongation [66]. In this case, it is possible that the limpet has stopped growing last winter, and winter temperatures are not reflected. Growth stops may have occurred by exceeding the thermal threshold or by ontogeny, affecting the correct reflection of winter and/or summer seasons, as it was previously observed for this same mollusk species at this latitude [67].

Regarding the LA-ICP-MS and CF-LIBS records, they show a significant correlation between them. Even though both series are very similar in each sample, some parts of the shell present notable differences in their concentration values. The ablated material, which is measured with LIBS and LA-ICP-MS, is not strictly the same because the second technique applied (LIBS) was measured on material some microns deeper than the material firstly ablated and measured by LA-ICP-MS [68]. This fact may lead to differences in spatial concentrations using both techniques. Regression coefficients (Fig. 7) were calculated in order to quantify the similarity between the concentrations obtained using both techniques applied and in every specimen. Regression coefficient values measured vary from $R^2 = 0.63$ to $R^2 = 0.81$. In addition, the averaged errors of calculated concentration by CF-LIBS in relation to the LA-ICP-MS values were obtained, resulting in 7.96% for LAN.563, 9.65% for LAN.565, 7.75% for LAN.566 and 9.84% for LAN.567.

3.4. Implications for paleoclimatology and archaeology

During the last two decades, several studies have highlighted the suitability of trace element analyses on biogenic marine mollusk shells as a high-resolution climate recorder [16,18,69]. In this context, LIBS technique has been presented as a rapid and low-cost methodology to measure elemental composition along the marine shell growth. The results obtained so far on different species have reported a significant correlation between Mg/Ca ratio value profiles along the shell growth and SST during the mollusks lifespan [36,37,45–47]. This suggests that this proxy could have very high implications for future paleoclimate and archaeological investigations.

Nevertheless, other studies have also shown that trace element ratio derived from mollusc shells as climate records also present a deep weakness. Hausmann et al. [45] and Lazareth et al. [70] have reported changes in elemental composition along isochronous growth lines/increments (i.e., layers deposited at the same time by the mollusks). Additional studies have also reported great variability in the elemental molar concentrations between very near growth lines/increments [65,71], which is a very relevant handicap for using trace element ratios as a suitable proxy to decipher environmental conditions during the past. Investigations previously conducted by Hausmann et al. [35,45] have shown that measuring all area of the shell section is very useful for better understanding how trace elements are incorporated within shell carbonate layers deposited at the same time. To conduct 2D measurement in the near future could be a very useful approach for accurately reconstructing SST during the past, since this novel method could allow us to obtain an average value for the same growth lines/increments (as other ICP based techniques offer). Additionally, to a better understanding of how carbonate is deposited by the mollusk will also enable us to determine the adequate measurement path along the shell growth for each species.

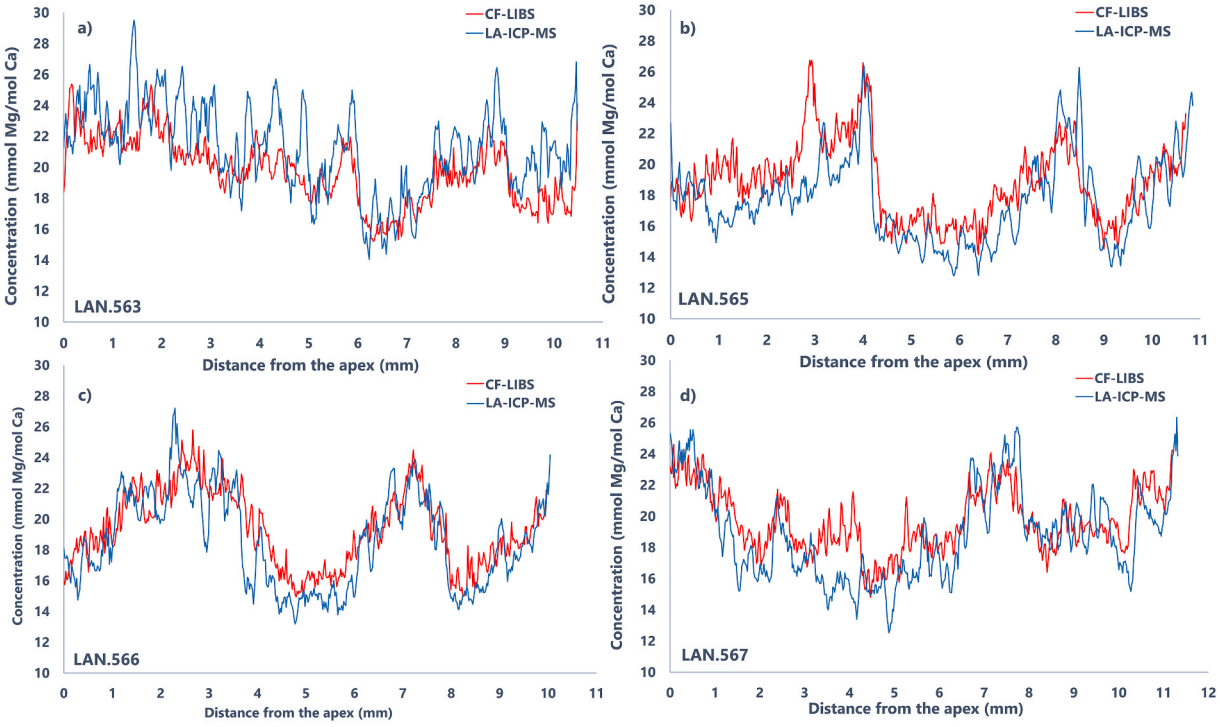

Fig. 6. CF-LIBS and LA-ICP-MS concentration profiles for the four limpet specimens.

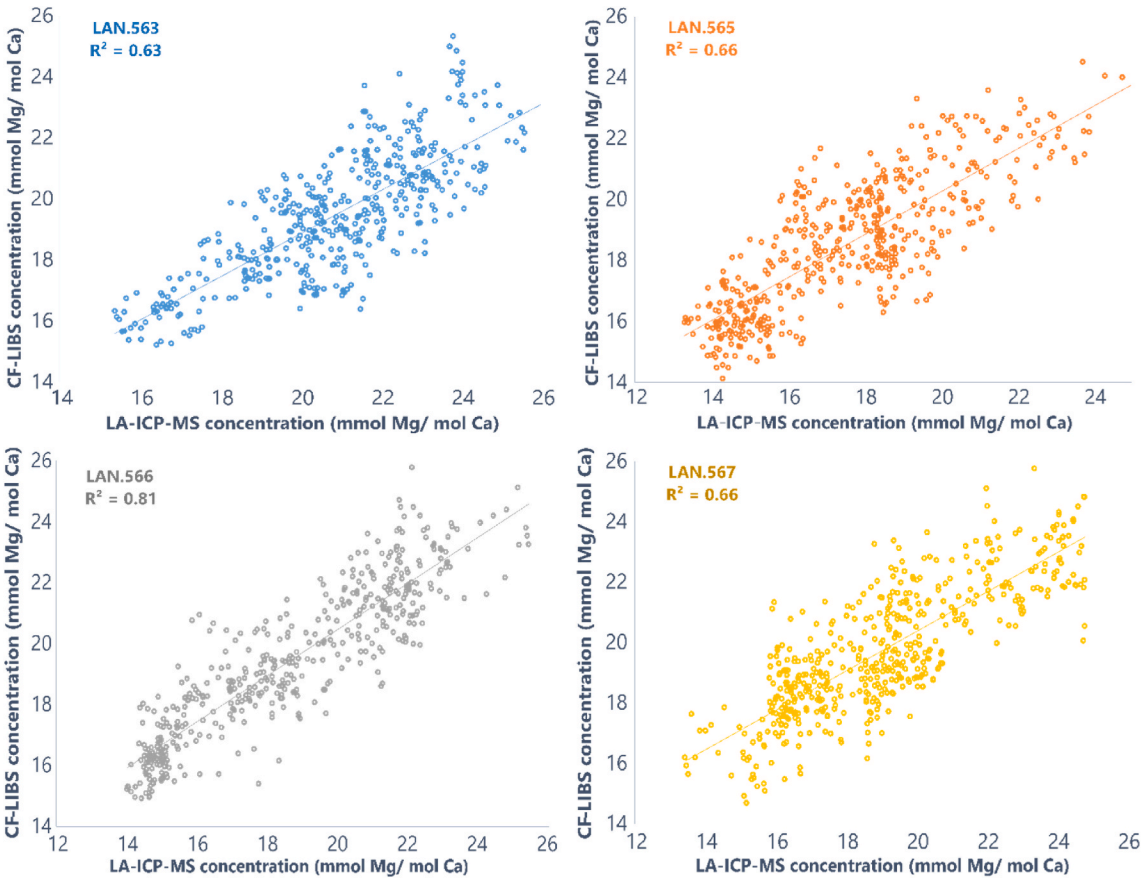

Fig. 7. Linear regression of CF-LIBS and LA-ICP-MS for the four specimens.

4. Conclusions

This study presents, for the first time, a comparative analysis of Mg/Ca concentration profiles measured within shells of the common limpet *P. depressa* using the LA-ICP-MS and CF-LIBS approaches. The Calibration-Free LIBS approach has been successfully applied to four *Patella depressa* limpet specimens. This method estimates molar concentrations of calcium and magnesium present in marine mollusk shells. Both methods identify expected trends in Mg/Ca concentration ratios in the edge of the shell (the most recently deposited material). Season of capture (i.e., end of summer) is correctly reflected in all 4 samples using both LA-ICP-MS and the CF-LIBS approach. However, LAN.563 specimen show a rather noisy sequence so that the winter and summer seasons previous to its collection cannot be clearly deduced. This behavior can be explained by the hypothesis that magnesium incorporation is influenced not only by temperature but also by physiological factors as well as the existence of intra-species variability or the existence of growth stops [63,64,72]. The results derived from this study show a relatively high correlation between the concentration data obtained with the LA-ICP-MS technique and CF-LIBS methodology, with regression coefficient values from 0.63 to 0.81 and average relative error values lower than 10% in every sample. The aforementioned metrics make the CF-LIBS approach a reliable way to determine Mg/Ca molar concentration within *P. depressa* limpet shells. The significant correlation observed between Mg/Ca profiles derived from both techniques have revealed, for the first time, that the algorithm used herein enables to correctly estimate the molar concentrations of the chemical elements in biogenic carbonates. CF-LIBS is a valuable approach for paleoclimatic and archaeological studies, yielding records of temperature seasonality during the life of an individual as well as the time of year when mollusks from archaeological sites were collected as a food resource by past human occupants. Nevertheless, as this study uses just four specimens, further studies are still required to further validate the approach.

Institutional Review Board statement

This investigation does not involve research on animal's transgenic small laboratory animals, animals transgenic farm animals, non-human primates or animals cloned farm animals. During the development of this study modern mollusk specimens were collected. The required authorizations were obtained from the Fishing Activity Service of the Cantabrian Government. The study was conducted according to the guidelines of the Declaration of Helsinki, and approved by the Institutional Review Board (or Ethics Committee) of Fishing Activity Service of the Cantabrian Government. Informed.

Credit author statement

Marina Martínez-Minchero: Conceptualization, Methodology, Investigation, Writing – Original Draft, Validation. Adolfo Cobo: Conceptualization, Methodology, Software, Writing - Original Draft, Validation. Ana Méndez-Vicente: Investigation, Writing - Review & Editing, Validation. Jorge Pisonero: Resources, Writing - Review & Editing, Validation. Nerea Bordel: Resources, Writing - Review & Editing, Validation. Igor Gutiérrez-Zugasti: Resources, Writing - Review & Editing, Validation. Patrick Roberts: Writing - Review & Editing, Validation. Álvaro Arrizabalaga: Writing - Review & Editing, Validation. José Valdiande: Investigation, Validation. Jesús Mirapeix: Investigation, Writing - Review & Editing. José Miguel López-Higuera: Supervision, Validation. Asier García-Escárzaga: Conceptualization, Methodology, Investigation, Supervision, Writing – Original Draft, Validation.

Declaration of competing interest

The authors declare that they have no known competing financial interests or personal relationships that could have appeared to influence the work reported in this paper.

Acknowledgments

This research was performed as part of the projects HAR2016-75605-R and HAR2017-86262-P funded by the Spanish Ministry of Economy and Competitiveness, MINECO. This work is also part of the projects PID2019-107270RB-C21 and MCI-21-PID2020-113951-GB-I00 funded by MCIN/AEI/10.13039/501100011033 and FEDER "A way to make Europe". This investigation was also supported by the Alexander von Humboldt Foundation thought a Humboldt Research Fellowship (no code available). This study is also part of the project PID2021-126937NB-I00 (PALEOCROSS) funded by MCIN/AEI/10.13039/501100011033 and by ERDF "A way of making Europe". MMM research was funded by predoctoral grant BES-2017-080076 from MINECO. During the development of this research AGE was funded by the Basque Country Postdoctoral Programme (grant number POS_2020_2_0032), by the University of La Rioja through a postdoctoral grant (no code available) and he is currently supported by the Catalonia Postdoctoral Programme through a Beatriu de Pinós fellowship (grant number 2020 BP 00240). This study has also been supported by the Prehistoric Research Consolidated Group of the Basque Country University (IT-1435-22), funded by the Basque Country Government. We would also like to thank the Max Planck Society for funding, as well as the Universidad de Cantabria (UC), Instituto Internacional de Investigaciones Prehistóricas de Cantabria (IIIPC), Grupo de Ingeniería Fotónica (GIF), University of the Basque Country (UPV/EHU) and University of La Rioja (UR) for providing support.

Appendix A. Supplementary data

Supplementary data to this article can be found online at https://doi.org/10.1016/j.talanta.2022.123757.

References

[1] I. Gutiérrez-Zugasti, S.H. Andersen, A.C. Araújo, C. Dupont, N. Milner, A. M. Monge-Soares Antonio M, Shell midden research in Atlantic Europe: state of the art, research problems and perspectives for the future, Quat. Int. 239 (2011) 70–85, https://doi.org/10.1016/j.quaint.2011.02.031.

[2] A.C. Colonese, M.A. Mannino, D.E. Bar-Yosef Mayer, D.A. Fa, J.C. Finlayson, D. Lubell, M.C. Stiner, Marine mollusc exploitation in Mediterranean prehistory: an overview, Quat. Int. 239 (2011) 86–103, https://doi.org/10.1016/j.quaint.2010.09.001.

[3] A.C. Colonese, S.A. Netto, A.S. Francisco, P. DeBlasis, X.S. Villagran, R. de Almeida Rocha Ponzoni, Y. Hancock, N. Hausmann, D.S. Eloy de Farias, A. Prendergast, B. R. Schöne, F.W. da Cruz, P.C.F. Giannini, Shell sclerochronology and stable isotopes of the bivalve Anomalocardia flexuosa (Linnaeus, 1767) from southern Brazil: implications for environmental and archaeological studies, Palaeogeogr. Palaeoclimatol. Palaeoecol. 484 (2017) 7–21, https://doi.org/10.1016/j.palaeo.2017.01.006.

[4] N. Hallmann, M. Burchell, B.R. Schöne, G.V. Irvine, D. Maxwell, High-resolution sclerochronological analysis of the bivalve mollusk Saxidomus gigantea from Alaska and British Columbia: techniques for revealing environmental archives and archaeological seasonality, J. Archaeol. Sci. 36 (2009) 2353–2364, https://doi.org/10.1016/j.jas.2009.06.018.

[5] T. Wang, D. Surge, S. Mithen, Seasonal temperature variability of the Neoglacial (3300–2500 BP) and Roman Warm Period (2500–1600 BP) reconstructed from oxygen isotope ratios of limpet shells (Patella vulgata), Northwest Scotland, Palaeogeogr. Palaeoclimatol. Palaeoecol. 317–318 (2012) 104–113, https://doi.org/10.1016/J.PALAEO.2011.12.016.

[6] B.R. Schöne, A.D. Freyre Castro, J. Fiebig, S.D. Houk, W. Oschmann, I. Kröncke, Sea surface water temperatures over the period 1884–1983 reconstructed from oxygen isotope ratios of a bivalve mollusk shell (Arctica islandica, southern North Sea), Palaeogeogr. Palaeoclimatol. Palaeoecol. 212 (2004) 215–232, https://doi.org/10.1016/J.PALAEO.2004.05.024.

[7] A. García-Escárzaga, I. Gutiérrez-Zugasti, A.B. Marín-Arroyo, R. Fernandes, S. Núñez De La Fuente, D. Cuenca-Solana, E. Iriarte, C. Simões, J. Martín-Chivelet, M.R. González-Morales, P. Roberts, Human forager response to abrupt climate change at 8.2 ka on the Atlantic coast of Europe, Sci. Rep. 12 (2022), https://doi.org/10.1038/s41598-022-10135-w.

[8] A. García-Escárzaga, I. Gutiérrez-Zugasti, A. Cobo, D. Cuenca-Solana, J. Martín-Chivelet, P. Roberts, M.R. González-Morales, Stable oxygen isotope analysis of Phorcus lineatus (da Costa, 1778) as a proxy for foraging seasonality during the Mesolithic in northern Iberia, Archaeol. Anthropol. Sci. 11 (2019) 5631–5644, https://doi.org/10.1007/s12520-019-00880-x.

[9] A.C. Colonese, S. Troelstra, P. Ziveri, F. Martini, D. Lo Vetro, S. Tommasini, Mesolithic shellfish exploitation in SW Italy: seasonal evidence from the oxygen isotopic composition of Osilinus turbinatus shells, J. Archaeol. Sci. 36 (2009) 1935–1944, https://doi.org/10.1016/J.JAS.2009.04.021.

[10] A.L. Prendergast, R.E. Stevens, T.C. O'Connell, A. Fadlalak, M. Touati, A. al-Mzeine, B.R. Schöne, C.O. Hunt, G. Barker, Changing patterns of eastern Mediterranean shellfish exploitation in the Late Glacial and Early Holocene: oxygen isotope evidence from gastropod in Epipaleolithic to Neolithic human occupation layers at the Haua Fteah cave, Libya, Quat. Int. 407 (2016) 80–93, https://doi.org/10.1016/J.QUAINT.2015.09.035.

[11] E.F. Owen, A.D. Wanamaker, S.C. Feindel, B.R. Schöne, P.D. Rawson, Stable carbon and oxygen isotope fractionation in bivalve (Placopecten magellanicus) larval aragonite, Geochem. Cosmochim. Acta 72 (2008) 4687–4698, https://doi.org/10.1016/J.GCA.2008.06.029.

[12] A.D. Wanamaker, K.J. Kreutz, H.W. Borns, D.S. Introne, S. Feindel, S. Funder, P. D. Rawson, B.J. Barber, Experimental determination of salinity, temperature. growth, and metabolic effects on shell isotope chemistry of Mytilus edulis collected from Maine and Greenland, Paleoceanography 22 (2007) 1–12, https://doi.org/10.1029/2006PA001352.

[13] D. Surge, T. Wang, I.G. Gutiérrez-Zugasti, P.H. Kelley, Isotope sclerochronology and season of annual growth line formation in limpet shells (patella vulgata) from warm- and cold-temperate zones in the eastern north Atlantic, Palaios 28 (2013) 386–393, https://doi.org/10.2110/palo.2012.p12-038r.

[14] C.F.T. Andrus, Shell midden sclerochronology, Quat. Sci. Rev. 30 (2011) 2892–2905, https://doi.org/10.1016/J.QUASCIREV.2011.07.016.

[15] M.J. Leng, J.P. Lewis, Oxygen isotopes in molluscan shell: applications in environmental archaeology, Environ. Archaeol. 21 (2016) 295–306, https://doi.org/10.1179/1749631414Y.0000000048.

[16] P.S. Freitas, L.J. Clarke, H. Kennedy, C.A. Richardson, The potential of combined Mg/Ca and δ 18O measurements within the shell of the bivalve Pecten maximus to estimate seawater δ 18O composition, Chem. Geol. 291 (2012) 286–293, https://doi.org/10.1016/j.chemgeo.2011.10.023.

[17] M. Elliot, K. Welsh, C. Chilcott, M. McCulloch, J. Chappell, B. Ayling, Profiles of trace elements and stable isotopes derived from giant long-lived Tridacna gigas bivalves: potential applications in paleoclimate studies, Palaeogeogr. Palaeoclimatol. Palaeoecol. 280 (2009) 132–142, https://doi.org/10.1016/j.palaeo.2009.06.007.

[18] J.E. Ferguson, Gideon Henderson, M.1P.S. Freitas, L.J. Clarke, H.A. Kennedy, C. A. Richardson, D.A. Fa, J.C. Finlayson, N.R. Charnley, Increased seasonality in the Western Mediterranean during the last glacial from limpet shell geochemistry, Earth Planet, Sci. Lett. 308 (2011) 325–333, https://doi.org/10.1016/J.EPSL.2011.05.054.

[19] S. Tynan, B.N. Opdyke, M. Walczak, S. Eggins, A. Dutton, Assessment of Mg/Ca in Saccostrea glomerata (the Sydney rock oyster) shell as a potential temperature record, Palaeogeogr. Palaeoclimatol. Palaeoecol. 484 (2017) 79–88, https://doi.org/10.1016/j.palaeo.2016.08.009.

[20] L.J. Cremers, David A. Radziemski, Handbook of Laser-Induced Breakdown Spectroscopy, John Wiley & Sons, 2006.

[21] S.W. Hudson, J. Craparo, R. De Saro, D. Apelian, Applications of laser-induced breakdown spectroscopy (LIBS) in molten metal processing, Metall. Mater. Trans. B Process Metall. Mater. Process. Sci. 48 (2017) 2731–2742, https://doi.org/10.1007/s11663-017-1032-7.

[22] H.K. Sanghapi, K.K. Ayyalasomayajula, F.Y. Yueh, J.P. Singh, D.L. McIntyre, J. C. Jain, J. Nakano, Analysis of slags using laser-induced breakdown spectroscopy, Spectrochim. Acta Part B At. Spectrosc. 115 (2016) 40–45, https://doi.org/10.1016/j.sab.2015.10.009.

[23] W.T.Y. Mohamed, Improved LIBS limit of detection of Be, Mg, Si, Mn, Fe and Cu in aluminum alloy samples using a portable Echelle spectrometer with ICCD camera, Opt Laser. Technol. 40 (2008) 30–38, https://doi.org/10.1016/j.optlastec.2007.04.004.

[24] V.K. Singh, Biomedical applications of laser induced breakdown spectroscopy, Horizons World Phys 287 (2016) 25–67, https://doi.org/10.1117/12.2080710.

[25] A. Kumar, F.Y. Yueh, J.P. Singh, S. Burgess, Characterization of malignant tissue cells by laser-induced breakdown spectroscopy, Appl. Opt. 43 (2004) 5399–5403, https://doi.org/10.1364/AO.43.005399.

[26] C.J.M. Lawley, A.M. Somers, B.A. Kjarsgaard, Rapid geochemical imaging of rocks and minerals with handheld laser induced breakdown spectroscopy (LIBS), J. Geochem. Explor. 222 (2021), 106694, https://doi.org/10.1016/j.gexplo.2020.106694.

[27] J. Chen, J. Pisonero, S. Chen, X. Wang, Q. Fan, Y. Duan, Convolutional neural network as a novel classification approach for laser-induced breakdown spectroscopy applications in lithological recognition, Spectrochim. Acta Part B At. Spectrosc. 166 (2020), 105801, https://doi.org/10.1016/J.SAB.2020.105801.

[28] C. Álvarez, J. Pisonero, N. Bordel, Quantification of fluorite mass-content in powdered ores using a Laser-Induced Breakdown Spectroscopy method based on the detection of minor elements and CaF molecular bands, Spectrochim. Acta Part B At. Spectrosc. 100 (2014) 123–128, https://doi.org/10.1016/j.sab.2014.07.024.

[29] K.K. Ayyalasomayajula, F. Yu-Yueh, J.P. Singh, D.L. McIntyre, J. Jain, Application of laser-induced breakdown spectroscopy for total carbon quantification in soil samples, Appl. Opt. 51 (2012) 149–154, https://doi.org/10.1364/AO.51.00B149.
[30] M. López-López, C. Alvarez-Llamas, J. Pisonero, C. García-Ruiz, N. Bordel, An exploratory study of the potential of LIBS for visualizing gunshot residue patterns, Forensic Sci. Int. 273 (2017) 124–131, https://doi.org/10.1016/j.forsciint.2017.02.012.
[31] A. Nevin, G. Spoto, D. Anglos, Laser spectroscopies for elemental and molecular analysis in art and archaeology, Appl. Phys. Mater. Sci. Process 106 (2012) 339–361, https://doi.org/10.1007/s00339-011-6699-z.
[32] K. Melessanaki, M. Mateo, S.C. Ferrence, P.P. Betancourt, D. Anglos, The Application of LIBS for the Analysis of Archaeological Ceramic and Metal Artifacts, vol. 198, 2002, pp. 156–163.
[33] S. Pérez-Diez, L.J. Fernández-Menéndez, H. Morillas, A. Martellone, B. De Nigris, M. Osanna, N. Bordel, F. Caruso, J.M. Madariaga, M. Maguregui, Elucidation of the chemical role of the pyroclastic materials on the state of conservation of mural paintings from pompeii, Angew. Chem., Int. Ed. 60 (2021) 3028–3036, https://doi.org/10.1002/anie.202010497.
[34] D.A. Cremers, R.C. Chinni, Laser-induced breakdown spectroscopy-capabilities and limitations, Appl. Spectrosc. Rev. 44 (2009) 457–506, https://doi.org/10.1080/05704920903058755.
[35] N. Hausmann, P. Siozos, A. Lemonis, A.C. Colonese, H.K. Robson, D. Anglos, Elemental mapping of Mg/Ca intensity ratios in marine mollusc shells using laser-induced breakdown spectroscopy, J. Anal. At. Spectrom. 32 (2017) 1467–1472, https://doi.org/10.1039/c7ja00131b.
[36] A. García-Escárzaga, L.J. Clarke, I. Gutiérrez-Zugasti, M.R. González-Morales, M. Martinez, J.M. López-Higuera, A. Cobo, Mg/Ca profiles within archaeological mollusc (patella vulgata) shells: laser-induced breakdown spectroscopy compared to inductively coupled plasma-optical emission spectrometry, Spectrochim. Acta Part B At. Spectrosc. 148 (2018) 8–15, https://doi.org/10.1016/j.sab.2018.05.026.
[37] A. García-Escárzaga, M. Martínez-Minchero, A. Cobo, I. Gutiérrez-Zugasti, A. Arrizabalaga, P. Roberts, Using mg/ca ratios from the limpet patella depressa pennant, 1777 measured by laser-induced breakdown spectroscopy (Libs) to reconstruct paleoclimate, Appl. Sci. 11 (2021), https://doi.org/10.3390/app11072959.
[38] M.B. Fricker, D. Günther, Instrumentation, Fundamentals, and Application of Laser Ablation-Inductively Coupled Plasma-Mass Spectrometry, 2016, pp. 1–19, https://doi.org/10.1007/978-3-662-49894-1_1.
[39] B. Hattendorf, C. Latkoczy, D. Günther, Laser ablation-ICPMS, Anal. Chem. 75 (2003) 341A–347A, https://doi.org/10.1021/ac031283r.
[40] J.S. Becker, H. Sela, J. Dobrowolska, M. Zoriy, J.S. Becker, Recent applications on isotope ratio measurements by ICP-MS and LA-ICP-MS on biological samples and single particles, Int. J. Mass Spectrom. 270 (2008) 1–7, https://doi.org/10.1016/J.IJMS.2007.10.008.
[41] S. Gao, X. Liu, H. Yuan, B. Hattendorf, D. Günther, L. Chen, S. Hu, Determination of forty two major and trace elements in USGS and NIST SRM glasses by laser ablation-inductively coupled plasma-mass spectrometry, Geostand. Geoanal. Res. 26 (2002) 181–196, https://doi.org/10.1111/j.1751-908x.2002.tb00886.x.
[42] J. Pisonero, B. Fernández, D. Günther, Critical revision of GD-MS, LA-ICP-MS and SIMS as inorganic mass spectrometric techniques for direct solid analysis, J. Anal. At. Spectrom. 24 (2009) 1145–1160, https://doi.org/10.1039/b904698d.
[43] J. Pisonero, H. Traub, B. Cappella, C. Álvarez-Llamas, A. Méndez, S. Richter, J. R. Encinar, J.M. Costa-Fernandez, N. Bordel, Exploring quantitative cellular bioimaging and assessment of CdSe/ZnS quantum dots cellular uptake in single cells, using ns-LA-ICP-SFMS, Talanta 227 (2021), https://doi.org/10.1016/j.talanta.2021.122162.
[44] B.E. Naes, S. Umpierrez, S. Ryland, C. Barnett, J.R. Almirall, A comparison of laser ablation inductively coupled plasma mass spectrometry, micro X-ray fluorescence spectroscopy, and laser induced breakdown spectroscopy for the discrimination of automotive glass, Spectrochim. Acta Part B At. Spectrosc. 63 (2008) 1145–1150, https://doi.org/10.1016/J.SAB.2008.07.005.
[45] N. Hausmann, A.L. Prendergast, A. Lemonis, J. Zech, P. Roberts, P. Siozos, D. Anglos, Extensive elemental mapping unlocks Mg/Ca ratios as climate proxy in seasonal records of Mediterranean limpets, Sci. Rep. 9 (2019) 1–10, https://doi.org/10.1038/s41598-019-39959-9.
[46] A. Cobo, A. García-Escárzaga, I. Gutiérrez-Zugasti, J. Setién, M.R. González-Morales, J.M. López-Higuera, Automated measurement of magnesium/calcium ratios in gastropod shells using laser-induced breakdown spectroscopy for paleoclimatic applications, Appl. Spectrosc. 71 (2016) 591–599, https://doi.org/10.1177/0003702816687570.
[47] A. García-Escárzaga, S. Moncayo, I. Gutiérrez-Zugasti, M.R. González-Morales, J. Martín-Chivelet, J.O. Cáceres, Mg/Ca ratios measured by laser induced breakdown spectroscopy (LIBS): a new approach to decipher environmental conditions, J. Anal. At. Spectrom. 30 (2015) 1913–1919, https://doi.org/10.1039/c5ja00168d.
[48] A. Ciucci, M. Corsi, V. Palleschi, S. Rastelli, A. Salvetti, E. Tognoni, New procedure for quantitative elemental analysis by laser-induced plasma spectroscopy, Appl. Spectrosc. 53 (1999) 960–964, https://doi.org/10.1366/0003702991947612.
[49] M. Fahad, Z. Farooq, M. Abrar, Comparative study of calibration-free laser-induced breakdown spectroscopy methods for quantitative elemental analysis of quartz-bearing limestone, Appl. Opt. 58 (2019) 3501, https://doi.org/10.1364/ao.58.003501.
[50] Z.A. Umar, N. Ahmed, R. Ahmed, U. Liaqat, M.A. Baig, Elemental composition analysis of granite rocks using LIBS and LA-TOF-MS, Appl. Opt. 57 (2018) 4985, https://doi.org/10.1364/ao.57.004985.
[51] M. Dell'Aglio, M. López-Claros, J.J. Laserna, S. Longo, A. De Giacomo, Stand-off laser induced breakdown spectroscopy on meteorites: calibration-free approach, Spectrochim. Acta Part B At. Spectrosc. 147 (2018) 87–92, https://doi.org/10.1016/j.sab.2018.05.024.
[52] M. Ferus, J. Koukal, L. Lenža, J. Srba, P. Kubelík, V. Laitl, E.M. Zanozina, P. Váňa, T. Kaiserová, A. Knížek, P. Rimmer, E. Chatzitheodoridis, S. Civiš, Calibration-free quantitative elemental analysis of meteor plasma using reference laser-induced breakdown spectroscopy of meteorite samples, Astron. Astrophys. 610 (2018), https://doi.org/10.1051/0004-6361/201629950.
[53] M. Corsi, G. Cristoforetti, M. Giuffrida, M. Hidalgo, S. Legnaioli, L. Masotti, V. Palleschi, A. Salvetti, E. Tognoni, C. Vallebona, A. Zanini, Archaeometric analysis of ancient copper artefacts by laser-induced breakdown spectroscopy technique, Microchim. Acta 152 (2005) 105–111, https://doi.org/10.1007/s00604-005-0388-6.
[54] V.S. Burakov, S.N. Raikov, Quantitative analysis of alloys and glasses by a calibration-free method using laser-induced breakdown spectroscopy, Spectrochim. Acta Part B At. Spectrosc. 62 (2007) 217–223, https://doi.org/10.1016/j.sab.2007.03.021.
[55] A. Marín Roldán, V. Dwivedi, J. Yravedra Sainz de los Terreros, P. Veis, Laser-Induced breakdown spectroscopy (LIBS) for the analyses of faunal bones: assembling of individuals and elemental quantification, Optik 218 (2020), https://doi.org/10.1016/J.IJLEO.2020.164992.
[56] R. Gaudiuso, M. Dell'Aglio, O. de Pascale, G.S. Senesi, A. de Giacomo, Laser induced breakdown spectroscopy for elemental analysis in environmental, cultural heritage and space applications: a review of methods and results, Sensors 10 (2010) 7434–7468, https://doi.org/10.3390/s100807434.
[57] C. Paton, J. Hellstrom, B. Paul, J. Woodhead, J. Hergt, Iolite: freeware for the visualisation and processing of mass spectrometric data, J. Anal. At. Spectrom. 26 (2011) 2508–2518, https://doi.org/10.1039/c1ja10172b.
[58] E. Tognoni, G. Cristoforetti, S. Legnaioli, V. Palleschi, Calibration-free laser-induced breakdown spectroscopy: state of the art, Spectrochim. Acta Part B At. Spectrosc. 65 (2010) 1–14, https://doi.org/10.1016/j.sab.2009.11.006.
[59] E. Grifoni, S. Legnaioli, M. Lezzerini, G. Lorenzetti, S. Pagnotta, V. Palleschi, Extracting Time-Resolved Information from Time-Integrated Laser-Induced Breakdown Spectra, 2014, https://doi.org/10.1155/2014/849310.
[60] H. Fu, Z. Ni, H. Wang, J. Jia, F. Dong, Accuracy improvement of calibration-free laser-induced breakdown spectroscopy, Plasma Sci. Technol. 21 (2019), 034001, https://doi.org/10.1088/2058-6272/aaead6.
[61] NIST Atomic Spectra Database, NIST Atomic Spectra Database, (n.d.). (https://physics.nist.gov/PhysRefData/ASD/lines_form.html).
[62] International Atomic Energy Agency, GENIE - General Internet Search Engine for Atomic Data, 2022. https://www-amdis.iaea.org/GENIE/.
[63] L.E. Graniero, D. Surge, D.P. Gillikin, I. Briz i Godino, M. Álvarez, Assessing elemental ratios as a paleotemperature proxy in the calcite shells of patelloid limpets, Palaeogeogr. Palaeoclimatol. Palaeoecol. 465 (2017) 376–385, https://doi.org/10.1016/J.PALAEO.2016.10.021.
[64] B.R. Schöne, Z. Zhang, P. Radermacher, J. Thébault, D.E. Jacob, E.V. Nunn, A. F. Maurer, Sr/Ca and Mg/Ca ratios of ontogenetically old, long-lived bivalve shells (Arctica islandica) and their function as paleotemperature proxies, Palaeogeogr. Palaeoclimatol. Palaeoecol. 302 (2011) 52–64, https://doi.org/10.1016/j.palaeo.2010.03.016.
[65] B.R. Schöne, Z. Zhang, D. Jacob, D.P. Gillikin, T. Tütken, D. Garbe-Schönberg, T. McConnaughey, A. Soldati, Effect of organic matrices on the determination of the trace element chemistry (Mg, Sr, Mg/Ca, Sr/Ca) of aragonitic bivalve shells (Arctica islandica) - comparison of ICP-OES and LA-ICP-MS data, Geochem. J. 44 (2010) 23–37, https://doi.org/10.2343/geochemj.1.0045.
[66] P.S. Freitas, L.J. Clarke, H.A. Kennedy, C.A. Richardson, Inter- and intra-specimen variability masks reliable temperature control on shell Mg/Ca ratios in laboratory- and field-cultured Mytilus edulis and Pecten maximus (bivalvia), Biogeosciences 5 (2008) 1245–1258, https://doi.org/10.5194/bg-5-1245-2008.
[67] A. García-Escárzaga, I. Gutiérrez-Zugasti, M.R. González-Morales, A. Arrizabalaga, J. Zech, P. Roberts, Shell sclerochronology and stable oxygen isotope ratios from the limpet Patella depressa Pennant, 1777: implications for palaeoclimate reconstruction and archaeology in northern Spain, Palaeogeogr. Palaeoclimatol. Palaeoecol. 560 (2020), 110023, https://doi.org/10.1016/J.PALAEO.2020.110023.
[68] S. Marali, B.R. Schöne, R. Mertz-Kraus, S.M. Griffin, A.D. Wanamaker, P.G. Butler, H.A. Holland, K.P. Jochum, Reproducibility of trace element time-series (Na/Ca, Mg/Ca, Mn/Ca, Sr/Ca, and Ba/Ca) within and between specimens of the bivalve Arctica islandica – a LA-ICP-MS line scan study, Palaeogeogr. Palaeoclimatol. Palaeoecol. 484 (2017) 109–128, https://doi.org/10.1016/J.PALAEO.2016.11.024.
[69] L. Bougeois, M. de Rafélis, G.J. Reichart, L.J. de Nooijer, F. Nicollin, G. Dupont-Nivet, A high resolution study of trace elements and stable isotopes in oyster shells to estimate Central Asian Middle Eocene seasonality, Chem. Geol. 363 (2014) 200–212, https://doi.org/10.1016/J.CHEMGEO.2013.10.037.
[70] C.E. Lazareth, F. Le Cornec, F. Candaudap, R. Freydier, Trace element heterogeneity along isochronous growth layers in bivalve shell: consequences for environmental reconstruction, Palaeogeogr. Palaeoclimatol. Palaeoecol. 373 (2013) 39–49, https://doi.org/10.1016/J.PALAEO.2011.04.024.
[71] S.R. Durham, D.P. Gillikin, D.H. Goodwin, G.P. Dietl, Rapid determination of oyster lifespans and growth rates using LA-ICP-MS line scans of shell Mg/Ca ratios, Palaeogeogr. Palaeoclimatol. Palaeoecol. 485 (2017) 201–209, https://doi.org/10.1016/j.palaeo.2017.06.013.
[72] A.D. Wanamaker, D.P. Gillikin, Strontium, magnesium, and barium incorporation in aragonitic shells of juvenile Arctica islandica: insights from temperature

controlled experiments, Chem. Geol. 526 (2019) 117–129, https://doi.org/10.1016/J.CHEMGEO.2018.02.012.